

Noise-based modelling of partially coherent radiation with frequency chirps

ANDREI TREBUSHININ^{1*}, GIANLUCA GELONI¹, AND SVITOZAR SERKEZ^{1*}

¹European XFEL, 4 Holzkoppel street, 22869 Schenefeld, Germany

*Corresponding authors: andrei.trebushinin@xfel.eu, svitozar.serkez@xfel.eu

Compiled January 12, 2024

We present a set of algorithms for modeling single instances of partially coherent radiation. These algorithms are based on approaches for simulating Gaussian Random Fields, where randomly generated noise is constrained by the effective radiation size in the conjugate Fourier domains. This approach, utilizing Fourier transform methods, significantly enhances computational efficiency compared to Monte-Carlo methods. The final result is a single stochastic instance of the field. With the proposed algorithms, one can simulate a variety of sources including but not limited to synchrotron and linear-regime free-electron laser radiation, thermal light. The resulting field is propagatable and can be further modeled as it passes through an optical scheme. We analytically confirmed that the results of the algorithms follow correct ensemble-averaged intensities and correlation functions. In addition, we presented simulations of use cases such as the simulation of the original double slit experiment and the simulation of free-electron laser radiation with frequency chirps. We also discuss in detail the possible limitations of our approach and proposed an extension of the generalized van Cittert-Zernike theorem. Furthermore, the algorithms provide illustrative examples ideal for teaching radiation coherence. © 2024 Optica Publishing Group

<http://dx.doi.org/10.1364/ao.XX.XXXXXX>

1. INTRODUCTION

[mention Fig. 1 before appearance...]

Simulations of partially coherent radiation play a pivotal role, enabling researchers to conduct comprehensive and cost-effective numerical experiments. This facilitates the design of optical systems and the testing of hypotheses without the constraints of physical experimentation. Advancements in synchrotron radiation (SR) sources [cite] and free-electron lasers (FELs) [cite] necessitate a more thorough description of sources using statistical optics approaches [1, 2]. Accelerator physics has pushed storage rings to their limits [cite], and radiation from such sources is predominantly partially coherent [cite]. In recent decades, free-electron laser facilities have emerged [cite], and the temporal statistical properties of Self-Amplified Spontaneous Emission (SASE) have proven to be very non-trivial [cite].

This highlights the significance of developing new simulation approaches to provide more versatile tools for studying radiation properties and propagate it thought the optical systems. In many scenarios, such as in the 3D simulation of FELs using tools like Genesis 1.3, numerical simulations are not just beneficial but often the only feasible method to comprehend the complex amplification processes that occur at FELs. In other situations, numerous parameters should be optimized before building a real-life facility. Overall, the trend toward start-to-end simulations and creating digital twins, combined with the

availability of ever-higher computational power, suggests that numerical simulations are becoming an increasingly important tool for studying physics and advancing our understanding of complex systems.

In our previous paper [3], we addressed the challenges associated with simulating partially coherent undulator radiation sources and the propagation of their radiation through optical systems. This algorithm can generally be described as shaping the field by multiplying white noise with restrictive distributions in both domains. The transformation to the inverse domain is performed by means of a fast Fourier transform, which ensures very high computational efficiency. Our proposal enables the representation of a partially coherent field as a single monochromatic instance of a statistical process – we exclusively considered Gaussian processes. This field can then be propagated using routine Fourier optics approaches and treated as a usual coherent field.

In this paper, we, at first, emphasize that such algorithms are not only applicable to synchrotron radiation and free-electron laser sources, which are our areas of expertise, but also more broadly to sources that exhibit stochastic properties. We begin by describing noise-based algorithms to simulate homogeneous/stationary fields, such as thermal sources of radiation, the cosmic microwave background [4], and applications beyond the traditional field of optics. These applications include highly

computationally efficient simulations of ocean waves for graphic design [5], as well as film grain simulations in modern cinematography [6]. A rigorous mathematical description of this algorithm is presented in [7]. Here, we present the algorithm itself and demonstrate a start-to-end simulation of the original Young's interference experiment based on this "homogeneous" algorithm.

We then discuss the simulation of quasi-homogeneous fields, as presented in [3], in the context of synchrotron radiation (SR) from undulators and for quasi-stationary free-electron laser (FEL) self-amplified spontaneous emission (SASE) radiation [8, 9]. Recently, we discovered that this approach has been extended [10] to encompass non-Gaussian statistics for simulating phenomena such as "ground motions and the fluctuating component of winds." This discussion aims to establish a foundation for a more general algorithm capable of simulating stochastic fields with frequency chirps.

For doing so, we utilize the Wigner function of the radiation to shape the field from white noise. The proposed algorithm is notable for its computational efficiency, relying on array-to-array multiplications, the generation of random samples, and the use Fourier-transform-type integrals. We demonstrate the practical application of these algorithms in a real-world scenario: self-amplified spontaneous emission (SASE) from free-electron lasers (FELs) in the presence of frequency chirps. Moreover, we explore the concept that the resulting field accurately represents a real field. We conclude our paper by discussing potential extensions of the proposed algorithms and addressing further challenges, such as going beyond Gaussian statistics and simulating inhomogeneous/nonstationary sources. In summary, we observe that noise-based simulations are extensively used in various fields of research and practical application, yet, to the best of our knowledge, they are less frequently applied in the optics community for simulating the stochastic properties of light.

2. COHERENCE OF RADIATION SOURCES

We shall now introduce a notation for describing the coherence properties of various sources. This is broadly applicable for various sources, but our focus will be on three specific sources: a thermal source, a synchrotron radiation source, and FEL SASE radiation. Each of these sources can be characterized as Gaussian random processes. And the key characteristic of such processes is that knowledge of the first-order correlation function allows for a full description of the process. This is because higher-order correlation functions can be deduced from the first-order one, a result stemming from the moment theorem in the context of statistical optics [1]. We will discuss that the numerical method we are proposing is versatile enough to be applicable to a broad range of sources sharing these statistical properties.

The definition of the correlation function of the first order is the following:

$$G(z, \vec{r}_1, \vec{r}_2, \omega_1, \omega_2) \equiv \langle \bar{E}(z, \vec{r}_1, \omega_1) \bar{E}^*(z, \vec{r}_2, \omega_2) \rangle, \quad (1)$$

or in normalized version:

$$g(\vec{r}_1, \vec{r}_2, \omega_1, \omega_2) = \frac{G(\vec{r}_1, \vec{r}_2, \omega_1, \omega_2)}{\sqrt{I(\vec{r}_1, \omega_1) I(\vec{r}_2, \omega_2)}}. \quad (2)$$

As soon as the process is Gaussian, Eq. 1 fully defines the statistical properties of the random process. Eq. 1 is fully general and we see that G depends both on coordinates (\vec{r}_1, \vec{r}_2) and frequencies (ω_1, ω_2) and this dependence can be very non-trivial.

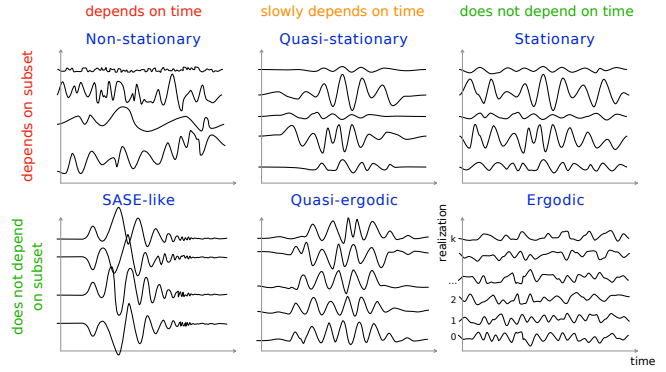


Fig. 2. Graphical illustration of process classifications based on their temporal stationarity and dependence on realizations. The top row depicts non-stationary, quasi-stationary, and stationary processes, demonstrating their type of dependence on time.

The bottom row illustrates SASE-like, quasi-ergodic, and ergodic processes, highlighting their non-dependence on specific realizations.

While random processes can exhibit highly variable behavior (Figs. 2, 3), we will focus on those with a certain degree of order. This order is manifested as consistency, either over time (stationarity) and/or across different instances (realizations) of the process. For SR sources and FELs radiation, it is practical to define a statistical realization of the process as a radiation emission by a single electron beam. These facilities typically operate at a specific repetition rate, and the properties of the electron beam are consistently reproducible within an experiment. Therefore, we can assert that the radiation properties of these sources are not dependent on a specific subset of realizations. It is important to note that while some processes may be fully stationary, others might be quasi-stationary or even non-stationary, as is the case with SASE FEL radiation. The variety of types of sources we depict in Fig. 2. We refer this non-stationary process while being not dependent on a realizations subset as SASE-like, which was introduced in [11].

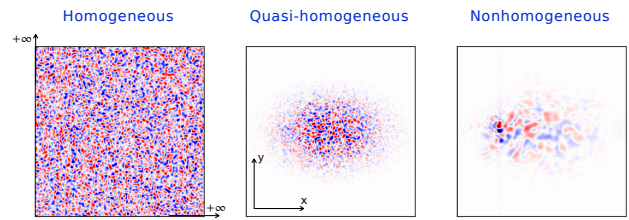


Fig. 3. Comparative visualization of coherence types across a spatial domain, showcasing homogeneous, quasi-homogeneous, and non-homogeneous patterns. The left image represents a uniformly distributed spikes of the radiation, such kind of radiation can be observed from thermal sources (e.g. Sun), the center image illustrates quasi-homogeneous type of distribution typical for synchrotron radiation sources, and the right image depicts a non-homogeneous distribution.

Not dependence on the chosen subset ensures that the spectral properties also do not depend on chosen realization. This gives us possibility to consider radiation in the frequency do-

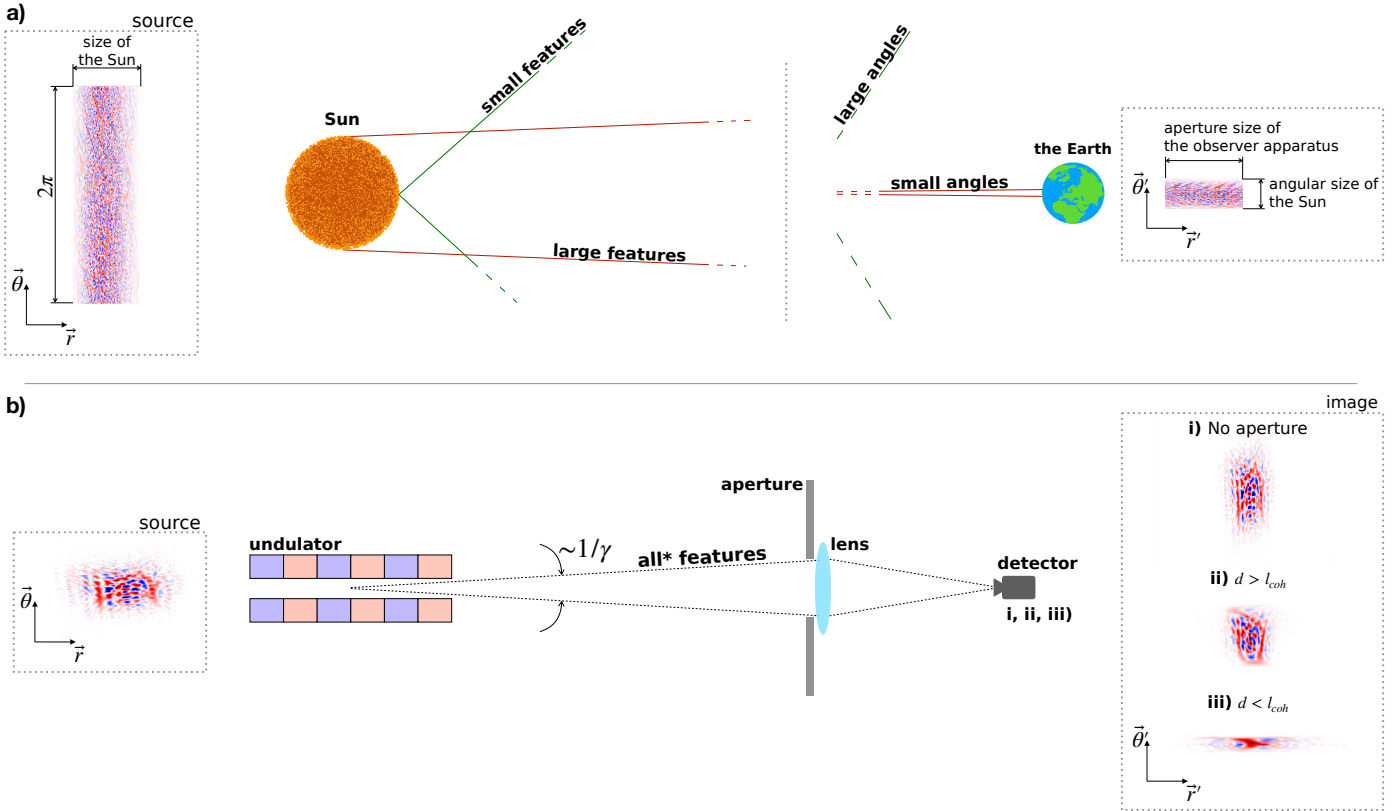


Fig. 1. (a) Incoherent radiation source – the Sun. The coherence length at the source is comparable to the wavelength dimension. The Sun exhibits various size features, ranging from the order of a wavelength to the Sun's own size. Smaller features diverge at larger angles, while larger features concentrate at smaller angles. The latter is captured in the correlation function in the far zone. To resolve smaller features, a larger aperture must be used at the observational plane. (b) Partially coherent source (undulator), an example of a quasi-homogeneous source. All features of the radiation are concentrated within an angle approximately equal to $\sim \gamma$. Such a source is described by the generalized van Cittert-Zernike theorem. The smallest features at the source are about the size of the coherence length of the source, which, after free space propagation, defines the radiation size in the far zone and the effective source size is transformed into the coherence length in the far zone.

main at the given frequency ω , i.e. through a perfect monochromator. In transverse plane Fig. 3, similar to longitudinal domain, radiation can be homogeneous, as the radiation from thermal sources, quasi-homogeneous, like SR radiation from an undulator and non-homogeneous. However, non-homogeneous sources requires more study in future works. Owing all complicity of the different types sources we will propose a generalized set of algorithms that can be applied not depending of the simulated domain. For this we at first define representation of quasi-stationary/homogeneous sources in mathematical form.

A. Quasi-homogeneous sources

The quasi-homogeneous sources are the large class of sources. In practice this means that the $\langle |\bar{E}(\vec{r})|^2 \rangle$ the radiation intensity varies slowly on the scale of the function $g(\vec{r}_1, \vec{r}_2)$. Here it is helpful to introduce another set of variables $(\vec{r}_1, \vec{r}_2) \rightarrow (\vec{r}, \Delta\vec{r})$, where $\vec{r} = (\vec{r}_2 + \vec{r}_1)/2$ and $\Delta\vec{r} = \vec{r}_2 - \vec{r}_1$. In practice, this kind of slow dependence means that $G(\vec{r}, \Delta\vec{r})$ function can be presented as the following:

$$G_\omega(\vec{r}, \Delta\vec{r}) \cong \sqrt{I_\omega(\vec{r}_1) I_\omega(\vec{r}_2)} g_\omega(\Delta\vec{r}), \quad (3)$$

where $I(\vec{r})$ is proportional to radiation intensity. In this representation the source is referred to be *quasi-homogeneous* [1]. We

consider this radiation seen thought a perfect monochromator and we denote it with \cdot_ω subscript. There is a spacial case when the source distribution is much larger than the coherence area. In this case we can further approximate Eq. 3:

$$G_\omega(\vec{r}, \Delta\vec{r}) \cong I_\omega(\vec{r}) g_\omega(\Delta\vec{r}), \quad (4)$$

This factorization is very helpful for proofing generalized van Cittert-Zernike theorem [1]

Another case follows from Eq. 4 when $g(\Delta\vec{r})$ is so small that it goes of order of the radiation wavelength. For most of practical calculations the studied system resolution is less than a wavelength and $g(\Delta\vec{r})$ can be approximated as Dirac delta function $\delta(\Delta\vec{r})$. So, we write $G(\vec{r}, \Delta\vec{r})$ in the following form:

$$G_\omega(\vec{r}, \Delta\vec{r}) \cong I_\omega(\vec{r}) \delta(\Delta\vec{r}), \quad (5)$$

This kind of sources are known as transversely incoherent sources. For both sources Eq. 4 and Eq. 5 one can show that the van Cittert-Zernike theorem [12, 13] and its generalized version holds [14, 15], namely that the modulus of the spectral degree of spatial coherence is equivalent to the two-dimensional Fourier transform of the source's intensity distribution. We have already presented an algorithm (SERVAL) [3], that sufficiently describes sources under Eq. 4. Here we would like to extend

145 this consideration further and provide analogues algorithms for
 146 sources Eq. 3 and Eq. 5.

147 B. Quasi-ergodic sources

148 We introduce that same representation of *quasi-ergodic* sources
 149 that *quasi-homogeneous* sources have with Eq. 3, Eq. 4 and Eq. 5
 150 but with variable ω instead of \vec{r} . This actually simplifies rep-
 151 resentation of the proposed algorithms and make it possible to use
 152 them not depending much on the simulated domain. As you can
 153 see that representation can be the same to the point of confusion.
 154 Actual fundamental reason for this is very similar numerical rela-
 155 tion between intensity distribution in one domain and coherence
 156 properties in the inverse domain, that is given by (generalized)
 157 van Cittert-Zernike theorem in spatial domain [12–15] and by
 158 Wiener-Khinchin theorem [cite] in temporal domain.

159 For the temporal properties of radiation we shall to assume
 160 that we observe radiation through a pinhole or spectral statistical
 161 properties of radiation does not varies much across transverse
 162 plane. For this purpose we denote complex degree of coherence
 163 and cross-spectral density as g_r and G_r , i.e. seen through a
 164 pinhole.

165 3. SIMULATION METHODS

166 In this section, we present a set of algorithms based on Eqs. 5, 4,
 167 and Eq. 3 that result in a single statistical realization of the field
 168 in the corresponding domain. For each algorithm, we present
 169 a formula along with a use case example. We also prove that
 170 the generated field adheres to the correct first-order correlation
 171 function as imposed, and that the power distribution follows a
 172 negative exponent as expected.

173 Before presenting the algorithms, it is necessary to discuss
 174 similar works based on the same approaches. Overall, there have
 175 been methods for simulating Gaussian Random processes with
 176 a given correlation function, as presented in a general form for
 177 incoherent sources in [7] and in application to simulations of the
 178 cosmic microwave background [16]. An algorithm for partially
 179 coherent radiation, specifically for chirp-less SASE radiation,
 180 was introduced in [9] and later corrected in [8]. We extend this
 181 consideration to SR undulator radiation [3]. In this paper, we
 182 aim not only to further extend it for radiation with chirps but
 183 also to provide a broader perspective on potential applications.
 184 As seen previously, it was often considered on a case-to-case
 185 basis, while we believe such an algorithm can be applied more
 186 broadly.

187 A. Incoherent sources

188 Cross-spectral density of the incoherent source can be expressed
 189 with Eq. 5 or its time-domain analogous. To shape the cor-
 190 rect instance of the field we generate complex Gaussian noise
 191 $\mathcal{N}(\vec{r}) = X(\vec{r}) + Y(\vec{r})$, where $X(\vec{r})$ and $Y(\vec{r})$ are normal distri-
 192 bution, and then we restrict this noise by source intensity distribu-
 193 tion, so:

$$\phi(\vec{r}) = \mathcal{F} \left\{ I\left(\frac{\vec{\xi}}{z_0}\right) \mathcal{N}\left(\frac{\vec{\xi}}{z_0}\right) \right\}(\vec{r}). \quad (6)$$

194 This equation is formulated for radiation at the observation
 195 plane (\vec{r}), located at a distance $z = z_0$ from the source. The
 196 source, positioned in the plane ($\vec{\xi}$) at $z = 0$, exhibits an intensity
 197 distribution $I\left(\frac{\vec{\xi}}{z_0}\right)$. Here, we essentially utilize the outcome of
 198 the original van Cittert-Zernike theorem, calculating the field
 199 already at the observation position. We could represent the field

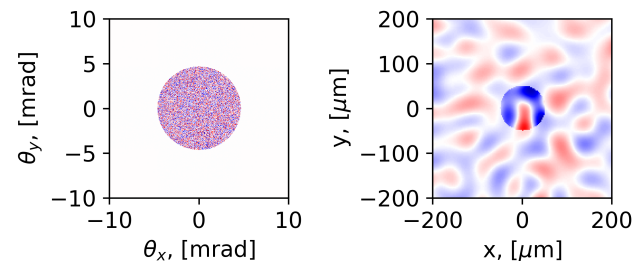


Fig. 4. (a) Sun intensity distribution at a given wavelength (500 μm) seen from the Earth. (b) Visible Sun radiation distribution at observation position. Such a source follows original van Cittert-Zernike theorem.

194 distribution at the source and then propagate it using a Fourier
 195 propagator to the far zone. However, propagating the entire
 196 incoherent field from the source is impractical, as incoherent
 197 sources radiate over a large solid angle. This would necessitate
 198 an immensely dense mesh of points to cover the inverse-space
 199 domain. Additionally, presenting the field at $z = z_0$ is logical in
 200 another sense: the observer typically has a certain acceptance
 201 opening, which effectively restricts the inverse space and elimi-
 202 nates the need to represent the entire inverse-space domain.

To proof that Eq. 6 correctly represent the field we can write its cross-correlation:

$$\begin{aligned} & \langle \phi(\vec{r}_1) \phi^*(\vec{r}_2) \rangle = \\ & \left\langle \iint_{\mathbb{R}^2} e^{\frac{2\pi i}{\lambda} ((\vec{r}_1 \cdot \vec{\theta}_1) - (\vec{r}_2 \cdot \vec{\theta}_2))} \sqrt{I(\vec{\theta}_1) I(\vec{\theta}_2)} \times \right. \\ & \left. \mathcal{N}(\vec{\theta}_1) \mathcal{N}^*(\vec{\theta}_2) d\vec{\theta}_1 d\vec{\theta}_2 \right\rangle \end{aligned} \quad (7)$$

Putting averaging inside the integral, accounting for property of the Gaussian noise $\langle \mathcal{N}(\vec{\theta}_1) \mathcal{N}^*(\vec{\theta}_2) \rangle = \delta(\vec{\theta}_2 - \vec{\theta}_1)$ and taking the integral we write:

$$\begin{aligned} & \langle \phi(\vec{r}_1) \phi^*(\vec{r}_2) \rangle = \\ & \int_{\mathbb{R}} e^{\frac{2\pi i}{\lambda} (\vec{\theta}_2 \cdot \Delta \vec{r})} I(\vec{\theta}_2) d\vec{\theta}_2 = G(z_0, \vec{r}_1, \vec{r}_2) \end{aligned} \quad (8)$$

203 where at the last step we used the van Cittert-Zernike theorem
 204 as all prerequisites of the theorem are satisfied.

205 This result is not surprising as one can recognise that we
 206 imprinted all the required statistical properties at the very begin-
 207 ning in Eq. 6. This algorithm is very efficient when on need to
 208 simulated an incoherent source on realization-to-realization ba-
 209 sis. And more importantly this algorithm is applicable to variety
 210 of incoherent sources, e.g. with this approach one can simulate
 211 cosmic microwave background [16], spatial distribution of radia-
 212 tion from a bending magnet, which is much close to our field
 213 of research or replicated Thomas Young's original experiment
 214 what we present in the next subsection.

215 A.1. Thomas Young's 1801' experiment

216 Here we would like to show practical application of the pro-
 217 posed algorithm for simulating interference experiment with in-
 218 coherent light. As for the example, we took the original Young's

experiment reported at Bakerian Lecture read on November 24, 1803. We provide the quote from his lecture to describe his experimental setup and then replicates it at a simulation:

"I made a small hole in a window-shutter, and covered it with a piece of thick paper, which I perforated with a fine needle. For greater convenience of observation, I placed a small looking glass without the window-shutter, in such a position as to reflect the sun's light, in a direction nearly horizontal, upon the opposite wall, and to cause the cone of diverging light to pass over a table, on which were several little screens of card-paper. I brought into the sunbeam a slip of card, about one-thirtieth of an inch in breadth, and observed its shadow, either on the wall, or on other cards held at different distances. Besides the fringes of colours on each side of the shadow, the shadow itself was divided by similar parallel fringes, of smaller dimensions, differing in number, according to the distance at which the shadow was observed, but leaving the middle of the shadow always white."

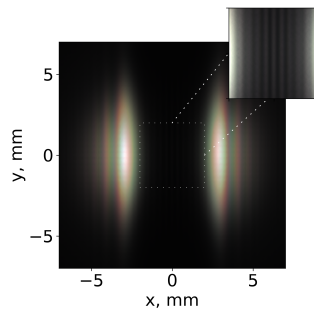


Fig. 5. Result of the original Young's interference experiment with a slip of cards. We observe colorful fringes and the shadow from the obstacle is divided by white parallel lines, while being visible only with increased exposure (here nearly ten time)

We replicated this experiment numerically assuming the distance from the window-shutter to the obstacle (a slip of card), which is [...] m and from it to one of the white screens – [...] m. The rest was replicated as described in the presented quote.

We present the results of this simulation in Fig. 5. For obtained colorful pattern of the diffraction we divided visible spectrum onto ten colors and simulated diffraction each on the "one-thirtieth-inch" obstacle separately. At the screen, we converted the resulting intensities into a red-green-blue representation and adjusted its colour appearance in Adobe Photoshop (white balance corrections, slight contrast adjustments, and saturation enchantment) to realistically represent what a human eye would see.

B. Partially coherent sources

We will present a new algorithm that accounts for chirps in radiation pulses but before we provide a discussion on the SERVAL algorithm that we presented in [3]. This we do for the sake of consistency of presentation as this algorithm is an intermediate step between Eq. 6 and the algorithm for chirped radiation.

Partially coherent source are those which have the coherence spot at the source large than the dimension of wavelength. This behaviour is usually the case in SR for both spatial and temporal domains and for temporal domain of FEL radiation. In

the case of transverse coherence of SR one should refer to the radiation formation length (L_f) which is always larger then the wavelength. Radiation diffraction size can always be written as $\sigma_r \sim (\lambda L_f)^{1/2}$ and in all cases are larger then wavelength. This ensure transverse coherence length is always large then wavelength and make the radiation to be partially coherent.

SR originates from relativistic beams and is narrowly confined in $\sim \gamma^{-1}$ angle which hint us that such noise distribution confinement by intensity distribution done in Eq. 6 should be done also in inverse space domain by effective radiation divergence. This results in what we called SERVAL algorithm for undulator radiation in [3].

B.1. Intensities-based approach

In the final results of the generalized van Cittert-Zernike theorem we see that $g(\Delta\vec{r})$ in the far zone is related with angular radiation distribution at the source via a Fourier transform as well as the source intensity distribution with the coherence cross-spectral density in the far zone, which is result of original theorem. We can apply this result in a similar manner to what we did for the incoherent radiation case with Eq. 6. By restricting the inverse space distribution by the effective radiation divergence, we can shape a partially coherent radiation. This approach yields the following expression:

$$\phi(\vec{r}) = \mathcal{F}^{-1} \left\{ \sqrt{\hat{I}(\vec{\theta})} \mathcal{F} \left\{ \sqrt{\hat{I}(\vec{r}')} \mathcal{N}(\vec{r}') \right\}(\vec{\theta}) \right\}(\vec{r}). \quad (9)$$

This equation is a result of our previous work in [3], where we demonstrated that Eq. 9 adheres to the correct first-order correlation function, which is sufficient to fully describe the stochastic process. Moreover, the form of Eq. 9 helps us recognize that this equation contains a factorized Wigner function distribution, consisting of $\hat{I}(\vec{\theta})$ and $\hat{I}(\vec{r})$. This insight enables us to derive an equation that accounts for radiation chirps. However, instead of using intensities, we will employ a Wigner function-based approach to represent the field.

B.2. Wigner-function-based approach

In the section we look at the temporal domain as would like to show a simulation of SASE FEL radiation. This radiation resulted from the electron beams with energy chirps [17, 18], and the basically replicate the electron beam chirp within the lasing window. As we said we will shape such radiation features using Wigner function. The definition for which is the following in time domain:

$$W(t, \omega) = \frac{1}{2\pi} \int_{-\infty}^{\infty} d(\Delta\omega) G_r(\omega, \Delta\omega) e^{-i\Delta\omega t}. \quad (10)$$

Now we shape a single instance of a field in the same manner as we did before in Eq. 9:

$$\phi(\omega) = \int_{-\infty}^{\infty} \sqrt{W(\omega, t)} \mathcal{N}(t) e^{i\omega t} dt. \quad (11)$$

We note that that we use the direct expression for the integral instead of Fourier transform as Wigner function depends also on ω . We visualize this algorithm in Fig. 6

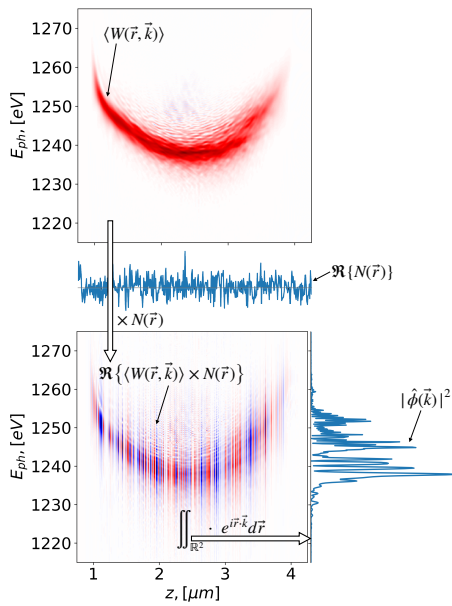


Fig. 6. [correct variables to ω and t] Visualization of the Wigner-function-based algorithm. A known Wigner function should be multiplied by the complex white noise and then a Fourier-like integral should be taken. The result is a single instance of the radiation spectrum.

This algorithm, in essence, does not differ much from those already presented. For all of them, the statistical properties of the process must be known in advance. This becomes apparent when we examine Eqs. 6 and 9, taking into account that we have utilized the van Cittert-Zernike theorem. Therefore, it either requires knowledge of the intensity distribution and an assumption of the applicability of the theorem, or direct knowledge of the correlation function. Similarly, in the case of the Wigner-function-based approach, as soon as the correlation function is known, one can calculate $W(t, \omega)$.

As always we need to cross-check if the emulated field by Eq. 11 represent correct cross-spectral density function. We write the correlation as the following:

$$\begin{aligned} \langle \phi(\omega_1)\phi^*(\omega_2) \rangle = \\ \left\langle \iint_{\mathbb{R}^2} e^{i(\omega_1 t_1 - \omega_2 t_2)} \sqrt{W(\omega_1, t_1)W(\omega_2, t_2)} \times \right. \\ \left. \mathcal{N}(t_1)\mathcal{N}^*(t_2) dt_1 dt_2 \right\rangle, \end{aligned} \quad (12)$$

Note that we imposes $W(\omega, t) \geq 0$. And here for convenience of Wigner function representation we changed variables: $(t_1, t_2) \rightarrow (\bar{t}, \Delta t)$. Also, as we did before, we make use the delta function property $\langle \mathcal{N}(\bar{t} + \frac{\Delta t}{2})\mathcal{N}^*(\bar{t} - \frac{\Delta t}{2}) \rangle = \delta(\Delta t)$ and write the following integral:

$$\begin{aligned} \langle \phi(\omega_1)\phi^*(\omega_2) \rangle = \\ \int_{\mathbb{R}} e^{i\bar{t} \cdot \Delta\omega} \sqrt{W(\omega_1, \bar{t})W(\omega_2, \bar{t})} d\bar{t} \end{aligned} \quad (13)$$

If we disclose the definition of the Wigner function and assume

that $\hat{G}(\bar{t}, \Delta t) = I(\bar{t})\hat{g}(\Delta t)$:

$$\begin{aligned} \left\langle \phi(\omega_1)\phi^*(\omega_2) \right\rangle = \\ \int_{\mathbb{R}^2} I(\bar{t})e^{i\bar{t}\Delta\omega} d\bar{t} \times \\ \sqrt{\int_{\mathbb{R}^2} \hat{g}(\Delta t_1)e^{i(\bar{\omega}+\Delta\omega)\Delta t_1} d(\Delta t_1)} \times \\ \sqrt{\int_{\mathbb{R}^2} \hat{g}(\Delta t_2)e^{i(\bar{\omega}-\Delta\omega)\Delta t_2} d(\Delta t_2)}. \end{aligned} \quad (14)$$

Using Van Cittert-Zernike theorem for each integral we end up with:

$$\left\langle \phi(\omega_1)\phi^*(\omega_2) \right\rangle = g(\Delta\omega) \sqrt{I(\bar{\omega} + \Delta\omega)I(\bar{\omega} - \Delta\omega)}. \quad (15)$$

It is clear that Eq. 11 is only approximate, but we will demonstrate the use of this algorithm to imitate real chirped SASE pulses in the following subsection

B.3. Numerical example: FEL SASE chirped radiation

We simulated a chirped pulse of SASE radiation in linear regime with Genesis 1.3 v2 code [19]. We deliberately stayed in the linear regime as when saturation is reached statistical properties of SASE radiation start to change differ for Gaussian statistics [20] [cite more], while Eq. 11 strictly implies Gaussian process. We used the output of the Wigner function from the Genesis 1.3 v2 simulation to feed-in the algorithm and then we generated the whole new ensemble of statistical realizations. Our expectation is that the averaged Wigner function will be the same one as the input, this would ensure correct statistical representation of each single instance of the simulated field: this is what we compare in Fig. 7

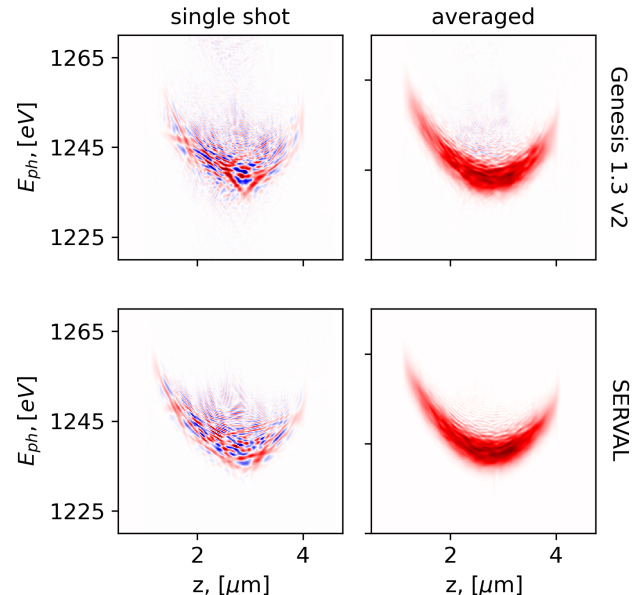


Fig. 7. [seemingly single shot Genesis result is slightly shorter, something to do with xlim] The first row is the results of the Genesis 1.3 v2 simulation Wigner function distributions are presented for a single shot event and ensemble-averaged distributions. The second row represents the emulated field resulting from the averaged Wigner function distribution.

313 Then we cross-check statistics of the resulted field if it still
 314 follows Gaussian one after all those mathematical operation, the
 315 results of this comparison we present in Fig. 8.

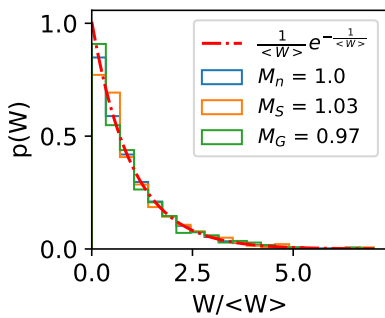


Fig. 8. Histogram of the power distribution of the radiation seen through a perfect monochromator. With red dot-dashed line we show fit of the complex noise distribution, that is presented with blue. The histogram for the SERVAL field is presented with orange and histogram distribution for Genesis 1.3 v2 output is presented with green color.

316 More often than not, the resulting correlation function of FEL
 317 SASE radiation is unknown, and there is no possibility to obtain
 318 it except by performing time-consuming simulations. Depend-
 319 ing on the task, one may use simpler models to work around
 320 this problem. In the case of SASE radiation, it is always true that
 321 the radiation chirp replicates the electron beam energy chirp.
 322 Once the natural SASE bandwidth is known, one can construct
 323 a surrogate Wigner distribution of the expected radiation. This
 324 can be a very effective approach for gathering data to train artifi-
 325 cial neural networks that perform electron beam chirp retrieval
 326 from measured spectral data.

327 4. DISCUSSION

328 The actual value of such a noise-based approach in simulating
 329 fields lies in its very high computational efficiency for simu-
 330 lating single instances. When comparing different approaches,
 331 a SERVAL-based approach has an order of magnitude advan-
 332 tage over Monte-Carlo-like approaches or mode decomposi-
 333 tion methods. Moreover, described approaches provide possi-
 334 bility to propagate each statistical realization as if it would be a
 335 coherent field, this also simplifies simulation routine for modeling
 336 partially coherent fields.

337 Simulating each instances separately is justified by the fact
 338 that a single monochromatic instance of a field is inherently
 339 coherent with itself. In other word, in an interference experiment,
 340 a single statistical realization will exhibit the highest degree of
 341 visibility. If it is considered as an end-result of an experiment
 342 one would conclude that that a complex coherence factor equals
 343 unity. However, by definition, the complex coherence factor is
 344 obtained as an average over a statistical ensemble. This implies
 345 that the field varies from realization to realization, resulting
 346 in a diffraction pattern – this would smear the final intensity
 347 distribution, and of course it will corresponds to a complex
 348 coherence factor significantly different from unity, as described
 349 in [1]. This leads to a simple yet important conclusion: a single
 350 statistical realization does not represent a partially coherent
 351 source by itself, but rather an ensemble of fields from this source.

352 To continue the discussion we find the relation between the
 353 approach based on simulating single instances and the coher-
 354 ent mode decomposition method. We consider coherent modes
 355 as the eigenfunctions of the homogeneous Fredholm integral
 356 equation of the second kind, where the kernel is the mutual
 357 spectral density (or cross-spectral density). To express a single
 358 instance of the field, one needs to sum up these eigenfunctions
 359 with random coefficients according to a specific rule [cite Man-
 360 del Wold]. The field generated in this manner is equivalent to
 361 the field produced by the proposed approaches or the Monte
 362 Carlo ones. This equivalence can be verified by calculating the
 363 cross-spectral density function and ensuring its consistency be-
 364 tween all mentioned methods. Therefore, the ensemble of these
 365 instances accurately describes the stochastic process.

366 5. CONCLUSION

367 In this paper we presented new algorithm for simulating radia-
 368 tion with chirps with a noise-based approach. Before introducing
 369 it we presented and explained two predecessor algorithms that
 370 utilize the same idea to start from complex Gaussian noise and
 371 then restrict this noise in direct and inverse domains. We showed
 372 analytically for the algorithm that it follows correct statistics and
 373 correlation function distribution. For the algorithms we pre-
 374 sented a use cases in particular it was the original double slit
 375 experiment and chirp SASE FEL radiation in linear regime. This
 376 approach we believe showed new way for simulating partially
 377 coherent radiation of different kinds: thermal sources, SR, and
 378 SASE FEL radiation, and we hope can also be applied for other
 379 kind of partially coherent sources the goes beyond of our exper-
 380 tise.

381 A. EXTENSION TO THE GENERALIZED VAN CITTERT- 382 ZERNIKE THEOREM

383 [a draft part] In this section we consider an extension to the
 384 generalized van Cittert-Zernike for the type of sources described
 385 with Eq. 3.

The proof of generalized van Cittert-Zernike theorem boils
 down to following integral:

$$G(z_0, \vec{r}, \Delta\vec{r}) = e^{-i\psi} \iint_{\mathbb{R}^2} G(0, \vec{r}, \Delta\vec{r}) e^{i(\Delta\vec{r} \cdot \vec{\xi} - \vec{r} \cdot \Delta\vec{\xi})} d\vec{\xi} d\Delta\vec{\xi}, \quad (16)$$

where $\psi = \dots$. Substituting $G(0, \vec{r}, \Delta\vec{r})$ from Eq. 3 we obtain:

$$G(z_0, \vec{r}, \Delta\vec{r}) = e^{-i\psi} \iint_{\mathbb{R}^2} \sqrt{I(r + \Delta r) I(r - \Delta r)} \times \\ g(\Delta r) e^{i(\Delta\vec{r} \cdot \vec{\xi} - \vec{r} \cdot \Delta\vec{\xi})} d\vec{\xi} d\Delta\vec{\xi}, \quad (17)$$

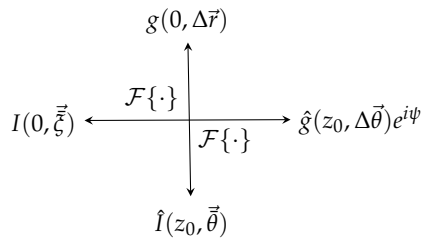
Then we expand I around r : $I(r \pm \Delta r) \approx I(r) + I'(r)\Delta r$ and
 substitute it in the integral:

$$G(z_0, \vec{r}, \Delta\vec{r}) = e^{-i\psi} \iint_{\mathbb{R}^2} \sqrt{I^2(r) - I'^2(r)\Delta r^2} \times \\ g(\Delta r) e^{i(\Delta\vec{r} \cdot \vec{\xi} - \vec{r} \cdot \Delta\vec{\xi})} d\vec{\xi} d\Delta\vec{\xi}. \quad (18)$$

Extracting $I^2(r)$ from the square root and expanding it assuming
 $I'^2(r)\Delta r^2 / I^2(r) \ll 1$ we obtain:

$$G(z_0, \vec{r}, \Delta\vec{r}) = e^{-i\psi} \iint_{\mathbb{R}^2} I(r) \left(1 - \frac{I'^2(r)\Delta r^2}{I^2(r)}\right) \times \\ g(\Delta r) e^{i(\Delta\vec{r} \cdot \vec{\xi} - \vec{r} \cdot \Delta\vec{\xi})} d\vec{\xi} d\Delta\vec{\xi}. \quad (19)$$

386 One may recognize that the first term in this integral is the result
 387 of the generalized van Cittert-Zernike theorem while the second
 388 term suppressed by square factor of Δr [?]. . .



389

Funding. No funding was received from any institution.

390 **Acknowledgements.** We thank Serguei Molodtsov for his interest in
 391 this work.

392 **Disclosures.** The authors declare no conflicts of interest.

393 **Data availability.** Data presented in this paper are generated with
 394 the OCELLOT toolkit [8].

REFERENCES

- 397 1. J. Goodman, *Statistical Optics*, Wiley Series in Pure and Applied Optics
 398 (Wiley, 2015).
- 399 2. G. Geloni, E. Saldin, E. Schneidmiller, and M. Yurkov, "Transverse
 400 coherence properties of X-ray beams in third-generation synchrotron
 401 radiation sources," *Nucl. Instruments Methods Phys. Res. Sect. A: Accel. Spectrometers, Detect. Assoc. Equip.* **588**, 463–493 (2008).
- 402 3. A. Trebuschini, G. Geloni, Y. Rakshun, and S. Serkez, "Gaussian random
 403 field generator for simulating partially coherent undulator radiation,"
 404 *Optica* **9**, 842 (2022).
- 405 4. G. Goon, "Cosmic Microwave Background simulations," (2021).
- 406 5. I. Pensionerov, "Fft-ocean," (2020).
- 407 6. I. Stephenson, "Simulating Film Grain using the Noise Power Spectrum,"
 408 Eurographics UK (2007).
- 409 7. A. Lang and J. Potthoff, "Fast simulation of Gaussian random fields,"
 410 *Monte Carlo Methods Appl.* **17** (2011). ArXiv: 1105.2737.
- 411 8. "Ocelot," URL: <https://github.com/ocelot-collab/ocelot>.
- 412 9. T. Pfeifer, Y. Jiang, S. Düsterer, R. Moshammer, and J. Ullrich, "Partial-
 413 coherence method to model experimental free-electron laser pulse
 414 statistics," *Opt. Lett.* **35**, 3441–3443 (2010). Publisher: Optical Society
 415 of America.
- 416 10. H. P. Hong, X. Z. Cui, and D. Qiao, "An algorithm to simulate nonstationary
 417 and non-Gaussian stochastic processes," *J. Infrastructure Preserv.
 418 Resil.* **2**, 17 (2021).
- 419 11. S. Serkez, "Design and Optimization of the Grating Monochromator
 420 for Soft X-Ray Self-Seeding FELs," Ph.D. thesis, Verlag Deutsches
 421 Elektronen-Synchrotron (2015). Number: PUBDB-2015-04348.
- 422 12. P. H. van Cittert, "Die Wahrscheinliche Schwingungsverteilung in Einer
 423 von Einer Lichtquelle Direkt Oder Mittels Einer Linse Beleuchteten
 424 Ebene," *Physica* **1**, 201–210 (1934).
- 425 13. F. Zernike, "The concept of degree of coherence and its application to
 426 optical problems," *Physica* **5**, 785–795 (1938).
- 427 14. J. Goodman, "Some effects of target-induced scintillation on optical
 428 radar performance," *Proc. IEEE* **53**, 1688–1700 (1965). Conference
 429 Name: Proceedings of the IEEE.
- 430 15. W. H. Carter and E. Wolf, "Coherence and radiometry with quasihomogeneous
 431 planar sources," *JOSA* **67**, 785–796 (1977). Publisher:
 432 Optica Publishing Group.
- 433 16. G. Goon, "Gaussian Fields," (2021).
- 434 17. S. Krinsky, "Frequency Chirped SASE FEL," Tech. Rep. SLAC-PUB-
 435 9633, 812615 (2003).
- 436 18. S. Serkez, O. Gorobtsov, D. E. Rivas, M. Meyer, B. Sobko, N. Gerasimova,
 437 N. Kujala, and G. Geloni, "Wigner distribution of self-amplified
 438 spontaneous emission free-electron laser pulses and extracting its
 439 autocorrelation," *J. Synchrotron Radiat.* **28**, 3–17 (2021). Number: 1
 440 Publisher: International Union of Crystallography.
- 441 19. S. Reiche, "Numerical studies for a single pass high gain free-electron
 442 laser," DESY-THESIS-2000-012; p. 177 p (1999).
- 443 20. E. Schneidmiller and M. Yurkov, "Statistical properties of the radiation
 444 from SASE FEL operating in a post-saturation regime with and without
 445 undulator tapering," *J. Mod. Opt.* **63**, 288–292 (2016).
- 446